Chaos, Solitons and Fractals 41 (2009) 843–853

Contents lists available at ScienceDirect

Chaos, Solitons and Fractals

journal homepage: www.elsevier.com/locate/chaos

From criticality to final collapse: Evolution of the "*b*-value" from 1.5 to 1.0

Alberto Carpinteri *, Giuseppe Lacidogna, Simone Puzzi

Politecnico di Torino, Department of Structural Engineering and Geotechnics, Corso Duca degli Abruzzi, 24, 10129 Torino, Italy

ARTICLE INFO

Article history:
Accepted 3 April 2008

ABSTRACT

Extensive research and studies on concrete fracture and failure by means of the acoustic emission (AE) technique have shown that fracture and damage growth can be characterized through a single synthetic parameter, namely the *b*-value, which changes systematically during the different stages of the failure process, as shown by several AE tests carried out from the specimen to the structural scale [Sammonds PR, Meredith PG, Murrel SAF, Main IG. Modelling the damage evolution in rock containing porefluid by acoustic emission. In: Proceedings of the Eurock'94; 1994; Colombo S, Main IG, Forde MC. Assessing damage of reinforced concrete beam using "*b*-value" analysis of acoustic emission signals. J Mater Civil Eng ASCE 2003;15:280–6; Carpinteri A, Lacidogna G, Niccolini G. Critical behaviour in concrete structures and damage localisation by Acoustic Emission. Key Eng Mater 2006;312:305–10]. This parameter can be linked to the value of the exponent α of the power-law distribution of the crack size in a damaged structure. In this paper, we propose a statistical interpretation for the variation of the *b*-value during the evolution of damage, based on a treatment originally proposed by [Carpinteri A. Mechanical damage and crack growth in concrete: plastic collapse to brittle fracture. Dordrecht: Martinus Nijhoff Publishers; 1986; Carpinteri A. Decrease of apparent tensile and bending strength with specimen size: two different explanations based on fracture mechanics. Int J Solid Struct 1989;25:407–29; Carpinteri A. Scaling laws and renormalization groups for strength and toughness of disordered materials. Int J Solid Struct 1994;31:291–302]. The proposed model captures the transition from the condition of criticality, in which $\alpha = 3$, to that of imminent failure, characterized by $\alpha = 2$, in terms of damage localisation.

1. Introduction

According to the definition from earthquake seismology [7], the magnitude in terms of AE technique is defined as follows:

$$m = \log_{10} A_{\max} + f(r), \tag{1}$$

where $A_{\max}$ is the signal amplitude, while $f(r)$ is a correction taking in account that the amplitude is a decreasing function of the distance r between the source and the sensor. In seismology, earthquakes of larger magnitude occur less frequently than earthquakes of smaller magnitude. This fact can be quantified in terms of an empirical magnitude-frequency relation, proposed by Gutenberg and Richter [7,8]:

$$\log_{10} N(\geqslant m) = a - bm \quad \text{or} \quad N(\geqslant m) = 10^{a-bm}, \tag{2}$$

where N is the cumulative number of earthquakes with magnitude $\geqslant m$ in a specified area and over a specified time interval, and b and a are positive constants varying from region to region. The empirical Eq. (2) has been tested

* Corresponding author. Tel.: +39 011 564 4850; fax: +39 011 564 4899.
E-mail address: alberto.carpinteri@polito.it (A. Carpinteri).

0960-0779/$ - see front matter © 2008 Elsevier Ltd. All rights reserved.
doi:10.1016/j.chaos.2008.04.010

successfully in the acoustic emission field to study the scaling of the "amplitude distribution" of AE waves [1–3]: this approach substantiates the similarity between the damage process in a structure and the seismic activity in the Earth's crust.

From Eq. (2), it can be seen that the b-value is the negative gradient of the log-linear AE frequency-magnitude diagram and hence it represents the slope of the amplitude distribution. The b-value changes systematically during the different stages of the failure process [1–3], and hence it can be used to estimate its development. In particular, recent results from AE laboratory tests on different types of specimens, as well as *in situ* AE investigations, show that the b-value is approximately equal to 1.5 at the condition of criticality, when the external load equals the peak load. In the later stages of damage evolution, when the final failure is imminent, the b-value tends to the unity [3]. It also seems that the minimum theoretical value for b could be one [1,2], although this is still an open issue.

By analogy with earthquakes, the AE damage *size-scaling* entails the validity of the relationship:

$$N(\geqslant L) = cL^{-2b}, \tag{3}$$

where N is the cumulative number of AE events generated by source defects with a characteristic linear dimension $\geqslant L$ and c is the total number of AE events. It is remarkable that the defect size distribution is a power-law with negative exponent $\alpha = 2b$, which can be interpreted as a fractal dimension of the damage domain [9,10]. Eq. (3), linking the b-value to the power-law exponent α, immediately allows to determine the evolution of the power-law exponent during the evolution of damage: at the condition of criticality $\alpha = 3$, whereas, during the later stages of damage evolution, when the final failure is imminent, the exponent α tends to 2.

To the best of the authors' knowledge, no modelling attempt has been made yet to describe or explain the variation of the b-value (or, equivalently, of the power-law exponent of the crack size distribution) and its link with the evolution in the fracture process. In this paper, we will provide a statistical interpretation to such a variation during the failure process by revisiting the original treatment proposed by Carpinteri [4–6].

As shown in several papers of the senior author starting from [4], this statistical approach is in close connection with the fractal geometry approach in the mechanics of damage and fracture of heterogeneous materials. Fractal geometry represents the natural tool to characterize self-organized processes, emphasizing their universality and the scaling laws arising at the critical points. Among the results obtained by the senior author, we could cite the modelling of the size-scale effects on strength, toughness [5,6,11,12] and critical strain [13] of heterogeneous materials and the optimization of the mechanical properties of advanced materials [14]. Further results include the development of an original fractional calculus-based framework for the analysis of materials with complex damage occurring in fractal domains [15] and the modelling of the scaling laws for fatigue [16] and friction [17]. Eventually, it is worthwhile recalling that the fractal geometry approach, together with Renormalization Group theory, has found an application also in seismology [18], that, as already remarked, is a field with strong analogies to material damage and fracture.

2. The self-similarity condition in bodies containing a multitude of cracks

Carpinteri [4–6] addressed the issue of the size-scale effects on the strength of bodies containing a multitude of imperfections on the basis of fracture mechanics and by means of a statistical analysis.

His aim was at interpreting the experimental trends of tensile strength and fracture toughness. Regarding the former, the experiments attested a scaling law for tensile strength characterized, in the strength vs. size bi-logarithmic plot, by the LEFM slope $-1/2$. In his analysis, Carpinteri started from the necessary condition for the scaling law to hold, i.e. the proportionality between the maximum defect size $a_{\max}$ and the structural linear size L, hereinafter called the self-similarity condition. Namely, if λ $(0 \leqslant \lambda \leqslant 1/2)$ is the power of the stress-singularity associated with the imperfections of the most dangerous shape, and if the probability density $p(a)$ of size distribution is such that the maximum size $a_{\max}$ is proportional to the linear scale L, then the strength size-scale effect in the σ_u vs. L bi-logarithmic plot is represented by a linear diagram with slope $-\lambda$ [4–6]. Given this condition, Carpinteri considered a set of similar bodies of different sizes containing a multitude of imperfections (cracks, voids, etc.) and determined the restrictive conditions on the form of the crack size distribution $p(a)$, which comply with self-similarity. He demonstrated that the probability density function of crack size must be a power-law:

$$p(a) = \frac{C}{a^{\alpha+1}}, \tag{4}$$

where C is a normalizing constant, such that the integral of $p(a)$ over the entire range of defect sizes, is equal to one. In what follows, we will revisit his demonstration and also confirm the obtained results by a completely different alternative demonstration.

Eventually, let us remark that the power-law distribution is particularly suited to describe the defect size in normal strength concrete, since in this material the interface between the matrix and the aggregates is the weakest link and the main source of initial defects. It may thus be assumed [19,20] that the statistics of the flaw sizes can be realistically represented by the statistics of grain diameters, and Stroeven [21] demonstrated that the power-law distribution of grain size exactly arises from the sieve curve used in the preparation of concrete.

2.1. Carpinteri's approach

Let us consider two different bodies in a scale ratio k; the smaller one of dimension L, the larger one of dimension kL, and let both bodies contain a multitude of imperfections coming from the same probability density function $p(a)$. Now, let us focus our attention on the smaller body; we can compute the value $\bar{a}$ of the defect size, such that, on average, one defect only (i.e. the largest) exceeds it. Let the material be uniform, so that we may define ρ as the mean (volumetric) density of defects. With this notation we obtain:

$$\Pr\{a \geqslant \bar{a}\}\rho L^3 \frac{1}{4\pi}\int_0^{2\pi}\int_0^{\pi} \sin\theta \,\mathrm{d}\theta\,\mathrm{d}\phi = 1, \tag{5}$$

ϕ and θ being the longitude and the latitude of the defect orientation. The factor $1/4\pi$ pertains to all imperfections, since all orientations are equally probable. The term $\Pr\{a \geqslant \bar{a}\}$ is graphically represented in Fig. 1a. As already stated, one defect only is expected to exceed the threshold $\bar{a}$ in a body of linear size L; its dimension, however, is still random, since we only know that this defect (which is obviously the largest defect in the body) is larger than the threshold: $a_{\max} \geqslant \bar{a}$.

Now we apply the same reasoning to the larger body, of size kL, by imposing the condition that one defect only exceeds the threshold $k\bar{a}$:

$$\Pr\{a \geqslant k\bar{a}\}\rho (kL)^3 \frac{1}{4\pi}\int_0^{2\pi}\int_0^{\pi} \sin\theta \,\mathrm{d}\theta\,\mathrm{d}\phi = 1 \tag{6}$$

And the term $\Pr\{a \geqslant k\bar{a}\}$ is shown in Fig. 1b. Equating Eqs. (5) and (6), the following relation is obtained:

$$\Pr\{a \geqslant \bar{a}\} = \Pr\{a \geqslant k\bar{a}\}k^3. \tag{7}$$

It is easy to see that Eq. (7) requires a cumulative probability of the defect size of the following form:

$$P(a) = 1 - \frac{K}{a^3}, \tag{8}$$

i.e. a power-law distribution. It must be observed that not the entire distribution must obey to the form of Eq. (8), but its tail only, since we are considering the behaviour of the extremes. In other terms, the probability density function has the following form:

$$p(a) = \frac{C}{a^4} \quad \text{for} \quad a \gg a_0, \tag{9}$$

which is valid only above some threshold a_0. The distribution in Eq. (9) has the same form as the self-similarity distribution in Eq. (4), with the exponent $\alpha = 3$.

More generally, if $\alpha \neq 3$, Carpinteri [4] suggested that the scaling of the maximum defect size (as a function of the body size b) for geometrical similar bodies in a scale ratio $k > 1$ may be written as:

$$a_{\max}(kL) = k^{\beta} a_{\max}(L). \tag{10}$$

As already stated, $a_{\max}$ is a random value exceeding the threshold $\bar{a}$, but now we also know that it is distributed according to the probability density function of Eq. (4) and, therefore, we can compute its expected value. The result shows that its expected value is proportional to the threshold $\bar{a}$ itself:

$$E(a|a \geqslant \bar{a}) \propto \frac{\alpha}{\alpha - 1}\bar{a}. \tag{11}$$

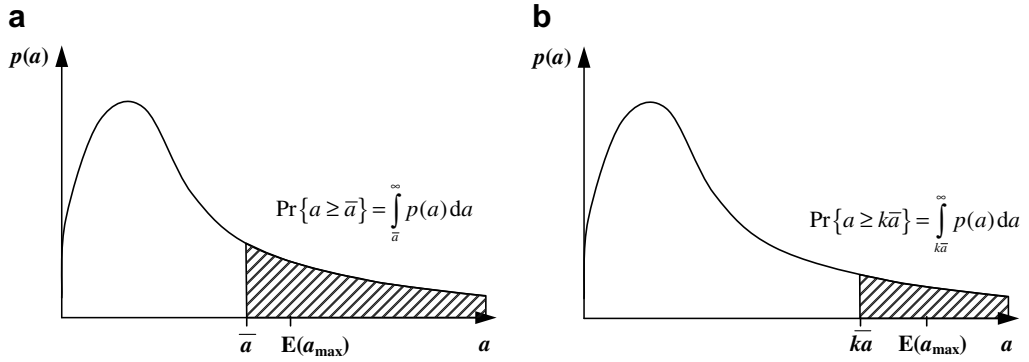

Fig. 1. Graphical representation of the probability integrals appearing in Eqs. (5) and (6), referring to a body of linear size L (a) and kL (b), respectively. Noticeably, not the whole distribution must be a power-law, but its tail only; the form of the distribution below some threshold a_0 does not affect the results of the present approach.

Since this is the expected value of the largest defect, $a_{\max} \propto \bar{a}$ and the scaling of $a_{\max}$ is also valid for $\bar{a}$; introducing Eq. (10) into Eq. (7) and replacing $\bar{a}$ with $a_{\max}$, we obtain:

$$[a_{\max}(L)]^{-\alpha} = [k^{\beta} a_{\max}(L)]^{-\alpha} k^3 \tag{12}$$

from which:

$$\beta = 3/\alpha. \tag{13}$$

This formula, describing the scaling of $a_{\max}$ with respect to the linear size L, comes as a refinement of the original result obtained by Carpinteri [4]:

$$\beta = 3/(\alpha + 1) \tag{14}$$

which is approximate for lower values of the exponent α and tends to the exact value for $\alpha \to \infty$. In particular, Eq. (13) confirms that the power-law exponent $\alpha = 3$ entails the condition of self-similarity.

2.2. Alternative demonstration

A completely different demonstration that the condition of self-similarity ($a_{\max}/L$ = constant on average) coupled with the condition of uniform damage in the body implies $\alpha = 3$, comes from the treatment proposed by Newman [22], in which the scaling between $a_{\max}$ and the number n of defects is obtained. If we take n defects distributed according to Eq. (4), the probability $\pi(a)\,\mathrm{d}a$ that the maximum falls in the interval $[a, a + \mathrm{d}a]$ can be computed by considering the compound probability that a single sample (say, the ith), will lie between a and $a + \mathrm{d}a$, and that all the others will be not greater: $p(a)\,\mathrm{d}a[P(a)]^{n-1}$, where $P(a)$ is the cumulative probability function:

$$P(a) = 1 - \frac{C}{\alpha a^{\alpha}}. \tag{15}$$

Then, we must consider that there are n ways to choose i, giving the probability:

$$\pi(a) = np(a)[P(a)]^{n-1}. \tag{16}$$

Now the mean value $E(a_{\max})$ of the largest sample can be computed as follows:

$$E(a_{\max}) = \int_{a_{\min}}^{\infty} a\pi(a)\,\mathrm{d}a = n\int_{a_{\min}}^{\infty} ap(a)[P(a)]^{n-1}\,\mathrm{d}a. \tag{17}$$

Introducing Eqs. (4) and (15) together with the normalization condition, which provides the value of the constant ($C = Na_{\min}^{\alpha}$), we have:

$$E(a_{\max}) = n\alpha\int_{a_{\min}}^{\infty} \left(\frac{a}{a_{\min}}\right)^{-\alpha}\left[1 - \left(\frac{a}{a_{\min}}\right)^{-\alpha}\right]^{n-1}\mathrm{d}a. \tag{18}$$

Setting the variable change $y = 1 - (a/a_{\min})^{-\alpha}$, we obtain:

$$E(a_{\max}) = na_{\min}\int_0^1 \frac{y^{n-1}}{(1-y)^{1/\alpha}}\,\mathrm{d}y = na_{\min}B\left(n, \frac{\alpha-1}{\alpha}\right), \tag{19}$$

where $B(n,m)$ is the Beta function:

$$B(n,m) = \int_0^1 (1-x)^{m-1}x^{n-1}\,\mathrm{d}x = \frac{\Gamma(n)\Gamma(m)}{\Gamma(n+m)}, \tag{20}$$

and $\Gamma(z) = \int_0^{\infty} t^{z-1}\mathrm{e}^{-t}\,\mathrm{d}t$ is the standard Gamma function. The Beta function has the interesting property that, for larger values of either of its arguments, it follows a power-law. For instance, for large n and fixed m, $B(n,m) \sim n^{-m}$. In our case, the number of defects n inside the body is large, so that we can write:

$$B\left(n, \frac{\alpha-1}{\alpha}\right) \sim n^{-\frac{\alpha-1}{\alpha}}, \tag{21}$$

and according to Eq. (19) the mean value of $a_{\max}$ scales as follows:

$$E(a_{\max}) \sim n^{1/\alpha}. \tag{22}$$

Now, if we introduce a constant volumetric density of defects ρ, the number of defects n in the body is proportional to the volume of the body itself: $n = \rho L^3$, and consequently the scaling of the mean value of $a_{\max}$ with respect to the linear size b is:

$$E(a_{\max}) \sim L^{3/\alpha}. \tag{23}$$

3. Experimental observations

Numerous experimental techniques have been employed to evaluate fracture processes, and a number of modelling approaches have been developed to predict fracture behaviour. The non-destructive method based on the acoustic emission (AE) technique has proved highly effective, especially to check and measure the damage phenomena that take place inside a structure subjected to mechanical loading.

The acoustic emission (AE) technique presents the potential for performing an effective monitoring of the integrity of Civil Engineering structures, from the laboratory to the structural scale, by means of a limited number of sensors. In this section an experimental investigation conducted on concrete and RC structures by means of the AE technique is described to confirm the theoretical treatment presented in Section 2. The AE signals reflecting the release of energy taking place during the damage process were recorded and microcracking sources were localized by measuring time delays through spatially distributed AE sensors.

In AE monitoring, piezoelectric (PZT) sensors are used, thereby exploiting the capacity of certain crystals to produce electric signals whenever they are subjected to a mechanical stress. The adopted equipment in this investigation consists of many units USAM®, that can be synchronized for multi-channel data processing. Each unit contains a preamplified wideband PZT sensor sensitive at the frequency range between 50 kHz and 800 kHz. The most relevant parameters acquired from the signals (arrival time, amplitude, duration, and number of oscillations) are stored in the USAMs memory and then downloaded to a PC for a multi-channel data processing. From this elaboration microcrack localisation is performed and the condition of the specimen can be determined [23,24].

3.1. In situ retrofitted RC beam test

Utilizing the AE technique, we have monitored and analysed a retrofitted RC beam with non-rectangular cross-section (Figs. 2 and 3). To improve its load carrying capacity and attenuate the effects of microcracking, the beam was reinforced

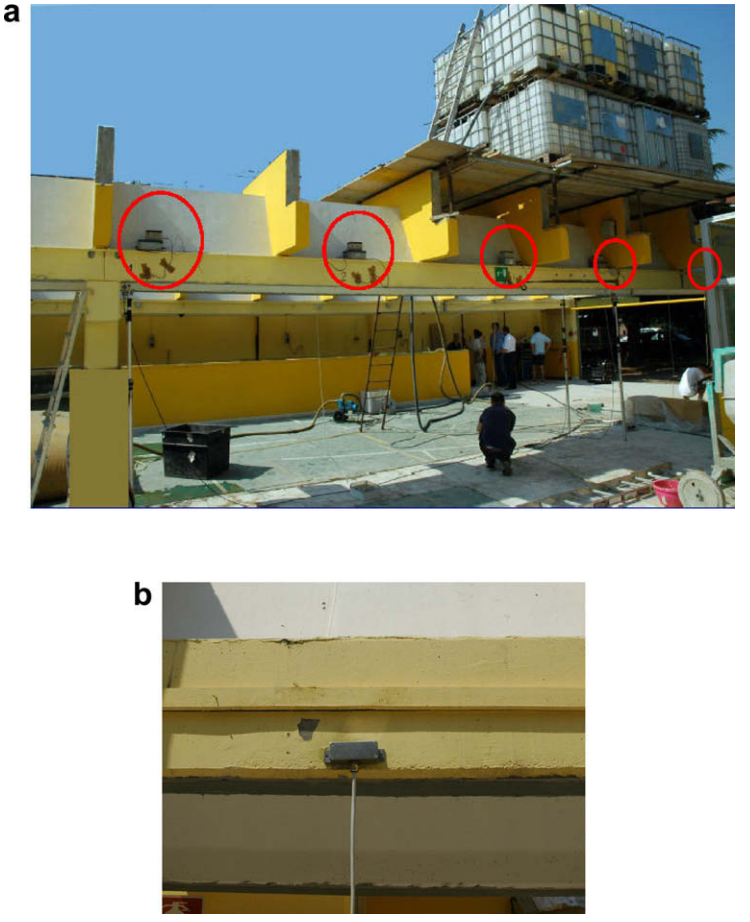

Fig. 2. *In situ* retrofitted RC beam test. (a) The structure during the loading test; circles denote the positions of the attached AE transducers. (b) Detail of an AE sensor applied on the lateral side of the beam.

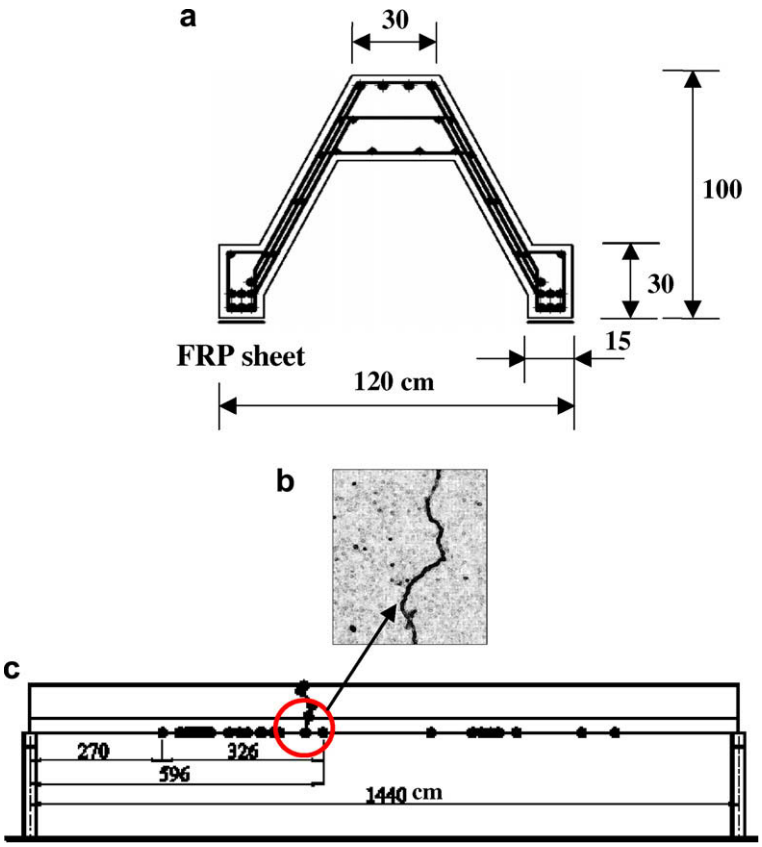

Fig. 3. *In situ* retrofitted RC beam test. (a) Scheme of the beam cross-section. (b) Photo of a flexural crack in between transducers 3 and 4 (using an optical microscopy with magnification 100X). (c) Scheme of the beam indicating localized AE sources.

externally with FRP sheets after the prior removal of the existing overload [23]. Then, an *in situ* loading test of the retrofitted beam was carried out.

The load has been applied by filling 16 vessels with water. Since each vessel had a capacity of 1000 l, a total vertical load of 160 kN was applied. The vessels were symmetrically positioned with respect to the center of the beam, covering a loading area of $4.00 \times 2.40 = 9.60\ m^2$ (see Fig. 2). Gradually filling the vessels, four loading steps of 40 kN per step were applied. After each step, the applied load was kept constant for 10 min. The whole loading test lasted approximately 3 h. A monitored mid-span deflection of 11 mm has been observed at the end of the loading test. The tested structure can be seen during the loading test in Fig. 2a, whereas, Fig. 2b reports a detailed view of an AE sensor placed on the opposite side of the beam.

During the test, five transducers (S_i) were applied on the two lateral faces of the beam. The AE source points were determined and are shown in Fig. 3c with black dots. In the loading range considered, micro-slips between the FRP sheets and concrete were not large enough to cause delamination. AE transducers, in fact, detected the onset of debonding only. The time evolution of the AE counting numbers, as detected by the AE transducers, is shown in Fig. 4a. Transducers 3 and 4 were close to flexural cracks and began to detect AE events from the beginning of the loading test. At the end of the test, they had detected the highest number of AE, followed by transducers 1 and 2, which were close to the beam supports.

This result is in agreement with the typical progression of cracking and collapse in retrofitted beams. Flexural cracks propagate upwards as loading progresses, but remain very narrow throughout the loading history. Delamination of the FRP sheets together with a thin layer of concrete takes place only when shear cracks develop in the proximity of the supports.

In addition to the crack localisation, the cumulative number of AE events with magnitudes greater than m as a function of m, was plotted on a semi-logarithmic scale. The final determination for the magnitude of an AE event is based on the average value of the results recorded by all the sensors. The reading of a single sensor is found using Eq. (1). From Fig. 4b a good agreement with the GR relationship is observed: the b-value is around 1.470.

3.2. Three-point bending test

The behaviour of a specimen subject to a three-point bending test was investigated at the laboratory scale. To determine the fracture process zone, AE generation was monitored. The specimen was a prism measuring $8 \times 15 \times 70\ cm^3$, with a

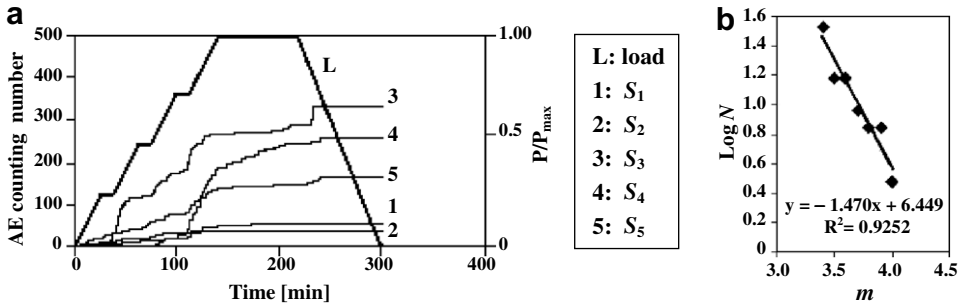

Fig. 4. (a) AE counting number for each sensor S_i during the loading test. (b) b-value during the loading test.

central 5 cm notch cut into it beforehand to ensure a centre crack. Five AE transducers were fitted to the specimen at points shown in Fig. 5a.

During the loading test, the source location procedure was successfully applied to identify the fracture process zone, as shown in Fig. 5a–c. Nucleation in the fracture process zone might be correlated with the AE clusters zone, and AE clusters are seen to propagate with increasing load [3,23]. The load vs. time curve for the specimen, characterizing the AE activity, is shown in Fig. 6a. In order to assess the ability of the AE technique to monitor the microscopic damages occurring inside the material and obtain information about the fracture processes, the load–time diagram, plotted for each second of the testing period, was broken down into three stages: a first stage (t_0, t_1) extending from the initial time to peak load, a second stage (t_1, t_2) going from peak load to the mainshock, and a third stage (t_2, t_f) going from the mainshock to the end of the process. In

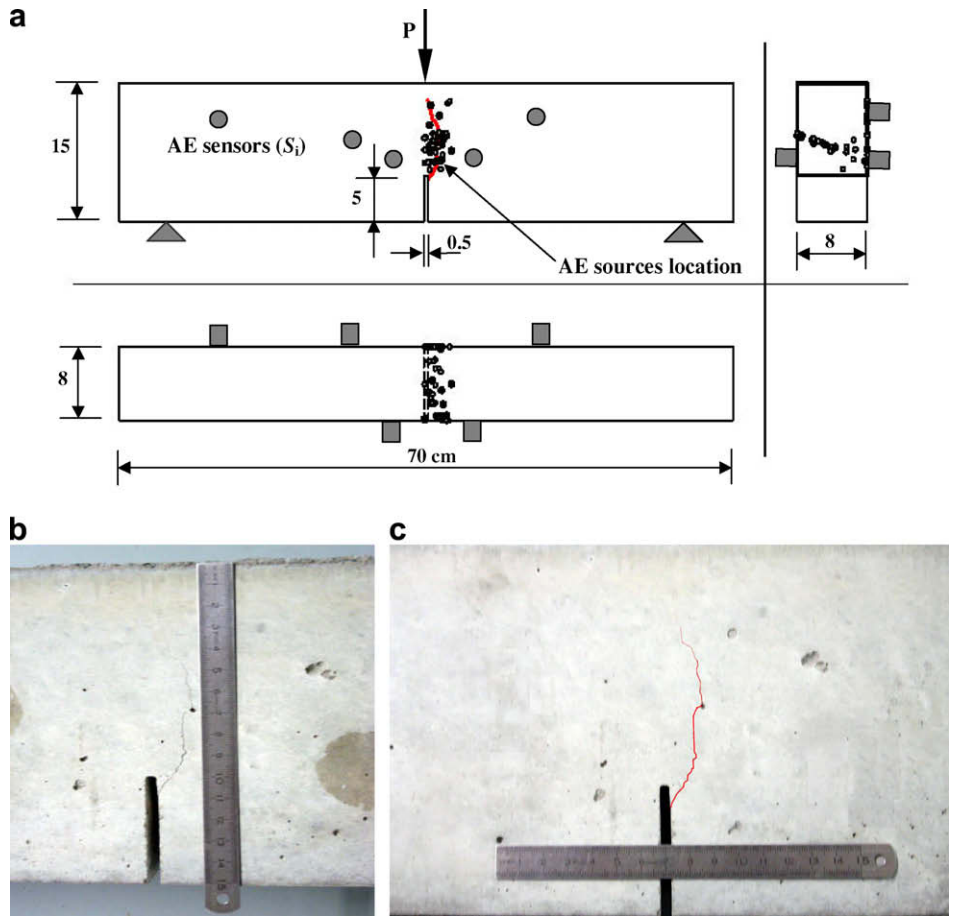

Fig. 5. Three point bending test. (a) Identification of the fracture process zone. (b) Zoom on the fracture process zone. (c) Process zone; the fracture is highlighted with a red line. (For interpretation of the references in color in this figure legend, the reader is referred to the web version of this article.)

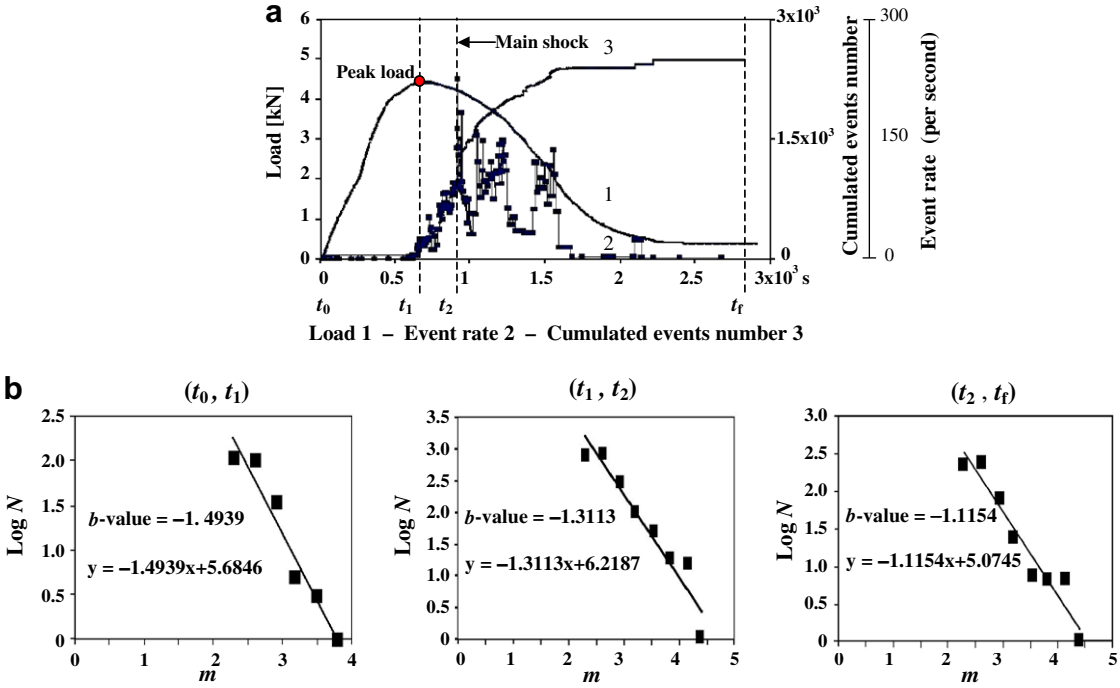

Fig. 6. Three point bending test. (a) Load vs. time curve and AE activity. (b) *b*-values during the loading test.

accordance with the GR law, *b*-values are shown for each stage in Fig. 6b. In this case too the *b*-values are seen to be in good agreement with the proposed approach: they range from 1.49 to 1.11. The lower value is obtained in the softening branch of the load–time curve, and it is very close to 1, as predicted in [4–6].

3.3. Concrete specimen in compression

Laboratory tests also analysed the behaviour of cylindrical concrete specimens in compression [25]. One of the 59 mm diameter specimens, with a height/diameter ratio $h/d = 2$, is shown in Fig. 7a. The compression test was performed in displacement control, by imposing a constant displacement rate at the upper loading platen. A displacement rate equal to 4×10^{-4} mm/s was adopted to obtain a very slow crack growth. The system adopted in the compression test utilizes rigid steel platens, the lateral deformation of concrete being, therefore, confined at the specimen ends, which are forced to have the same lateral deformation as the rigid platens. In this case, shear–stresses develop between specimen and loading platen, causing a three-dimensional state of stress at the specimen ends.

Compressive load vs. time, cumulated event number, and event rate (for each second of the testing period) are depicted in Fig. 7b. Also in this case, the load–time diagram was subdivided into three stages. The *b*-values obtained for each stage are shown in Fig. 7c; they range from 1.64 to 1.20. The lower value, rather close to 1, was obtained again in the softening branch of the load–time curve.

4. From criticality to final collapse: evolution of the power-law exponent α and of the *b*-value

The previous analysis, and particularly the result given by Eq. (13) (and confirmed by Eq. (23)), can provide insight into the evolution of the crack size population during the development of cracking and damage, allowing to interpret the experimentally observed variation of the *b*-value, which, as already stated (see Eq. (3)), is equal to $\alpha/2$.

At the condition of criticality, two main different mechanisms contribute to damage, i.e. fracture nucleation and fracture growth, whilst coalescence is still not active or, at least, not relevant. This remark is in agreement with experiments and analytical models proposed by researchers working on seismicity and fault size evolution (Spyropoulos et al. [26]). In the early phase of the loading process, when nucleation is the main mechanism, defects are likely to be spread uniformly in the whole body of the structure or in part of it, as shown in Fig. 8a, allowing us to define a mean volumetric density of defects ρ, so that the number of defects n in the body is proportional to the volume of the body itself: $n = \rho L^3$. We considered this case already: introducing this value into Eq. (22), we obtain the scaling of Eq. (23). To comply with the self-similarity condition, which guarantees that the size-scale effect holds, we necessarily obtain that $\alpha = 3$. By considering the proportionality relationship between α and the *b*-value, we get $b = 1.5$, which is in agreement with experimental findings [1–3]. In all the presented

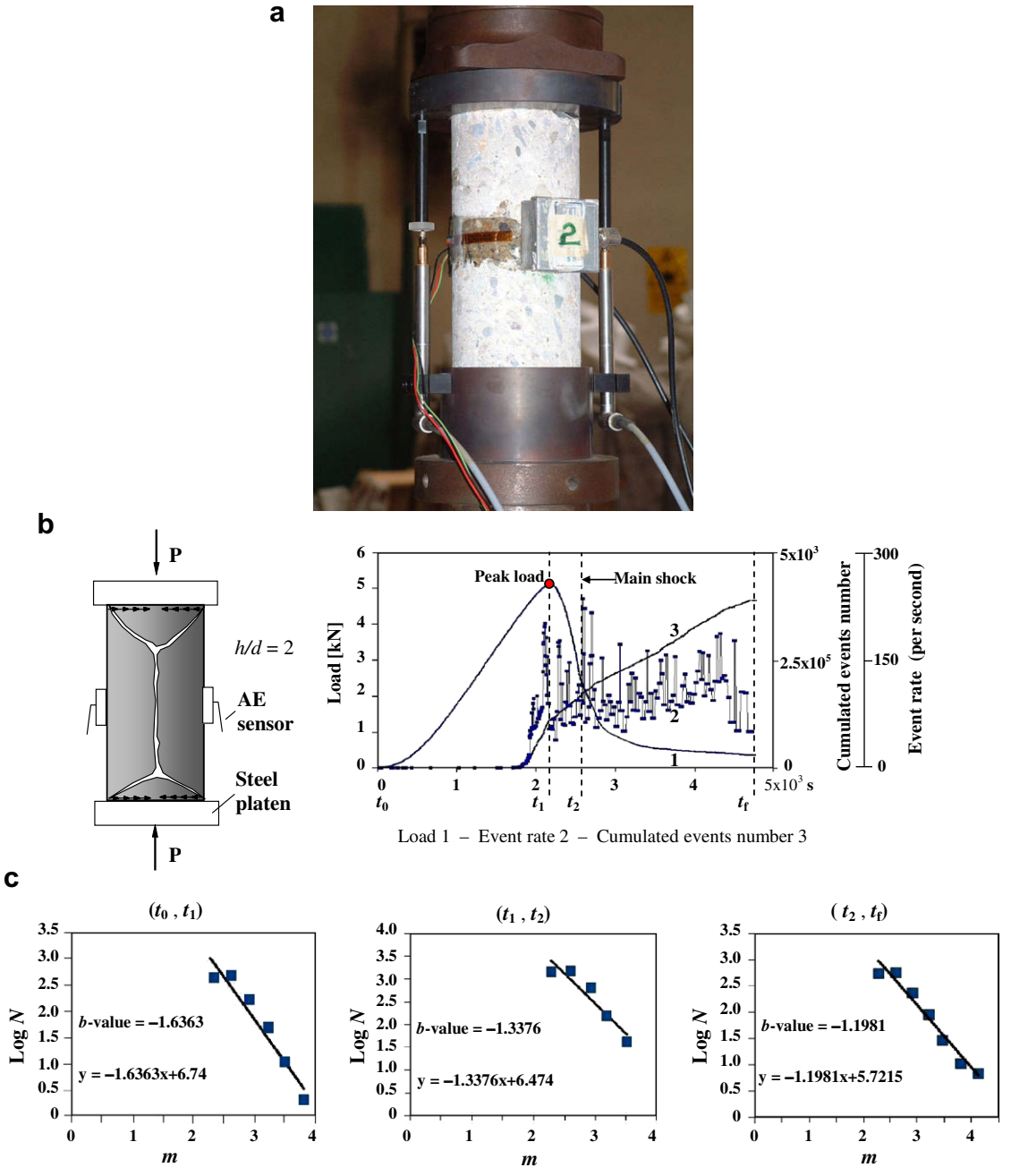

Fig. 7. Cylindrical concrete specimen in compression. (a) Testing set-up, with an AE sensor clearly visible on the lateral surface of the specimen. (b) Load vs. time curve and AE activity. (c) *b*-values during the loading test.

experiments, at the beginning of the loading process, when nucleation of cracks dominates, the obtained *b*-values are always between 1.5 and 2. This happens since initial microcracks are always evenly distributed, either in the whole structure under test – as in the case of the cylinder specimen in compression – or in part of it. This latter case applies to both the FRP retrofitted beam, where cracks naturally develop in a volume close to the interface between FRP sheet and beam soffit, and the three point bending specimen, where fracture should necessarily develop in the process zone near the initial notch.

At the condition of final collapse, when failure of the structure is imminent, the damaging process concentrates the majority of the cracks near the final failure surface [27], as shown in Fig. 8b; growth and coalescence are the main damage mechanisms and sharp localisation occurs. This hypothesis is strongly supported by AE tests [28], which allow to ascertain not only the evolution of the *b*-value through the analysis of the signal amplitude, but also the localisation of AE sources and the development of the microcracks inside the material, evidencing how they concentrate, after the critical phase, along

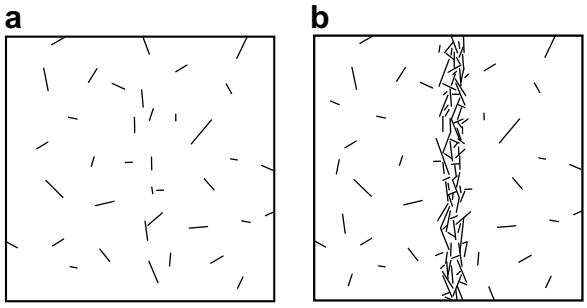

Fig. 8. (a) Criticality condition, with uniform damage in the bulk and (b) imminent failure, with damage concentrated in a narrow band around the final fracture surface.

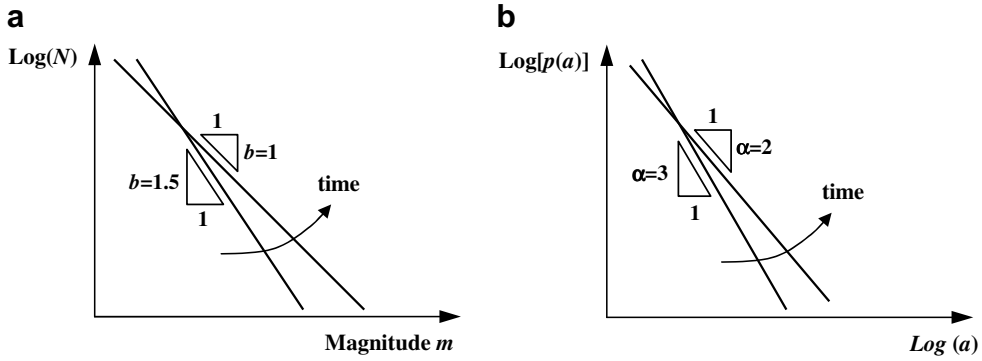

Fig. 9. (a) Experimental evidence of the evolution of the *b*-value on the GR-plot during AE testing and (b) theoretical evolution of the crack size distribution during the same test.

preferential paths (see, e.g., Fig. 5b). When such localisation occurs, a constant volumetric density of defects for the whole body or structure cannot be used consistently, since the majority of cracks is concentrated in a narrow band around the final fracture surface, whilst those outside this band can be considered negligible. In this case, the number of cracks has to be considered proportional to the size of the band around the fracture surface, and, therefore, to the square of the linear size: $n \sim L^2$. This hypothesis, inserted into Eq. (22), yields $E(a_{\max}) \sim L^{2/\alpha}$. Given this, for the self-similarity condition to hold, i.e. $E(a_{\max})/L$ = constant, it is necessary that the power-law exponent $\alpha = 2$. By considering again the proportionality relationship between α and the *b*-value, we obtain $b = 1$, which is the typical *b*-value when the structure failure is incipient [3]. The decrease towards 1 is clearly visible in Figs. 6b and 7c. The evolutions of the *b*-value and of the exponent α of the defect size distribution during a loading test follow the trends qualitatively sketched in Fig. 9. From a comparison of the two graphs it clearly appears that a decreasing *b*-value not only reveals an increase in damage, but also is a demonstration of the ongoing increase in crack sizes.

5. Conclusions

In this paper we revisited the statistical treatment proposed by Carpinteri [4–6], originally proposed to explain the statistical nature of the size-scale effect on the tensile strength of disordered materials containing many imperfections. Starting from imposing the condition of self-similarity, which is the only one complying with the size-scale effect observed in the experiments, we obtain at criticality, when damage in the body is still uniform and before localisation occurs, that the value of the power-law exponent is $\alpha = 3$. This value, which corresponds to $b = 1.5$, is in close agreement with AE experiments. Then, by considering the condition of imminent failure, characterized by strong damage localisation, we obtain from the self-similarity condition that $\alpha = 2$, which entails that $b = 1$, being also in agreement with the experimental findings. The proposed approach thus captures the transition from the condition of criticality to that of final collapse, allowing to give an interpretation to the variation of the power-law exponent (or of the *b*-value) in terms of damage localisation. The theoretical results are confirmed by experiments from AE laboratory tests on two different geometries, as well as from *in situ* AE investigations.

Acknowledgements

The financial support of the European Union to the Leonardo da Vinci Project I/06/B/F/PP-154069 "Innovative Learning and Training on Fracture (ILTOF)" is gratefully acknowledged.

References

[1] Sammonds PR, Meredith PG, Murrel SAF, Main IG. Modelling the damage evolution in rock containing porefluid by acoustic emission. In: Proceedings of Eurock'94; 1994.
[2] Colombo S, Main IG, Forde MC. Assessing damage of reinforced concrete beam using "*b*-value" analysis of acoustic emission signals. J Mater Civil Eng ASCE 2003;15:280–6.
[3] Carpinteri A, Lacidogna G, Niccolini G. Critical behaviour in concrete structures and damage localization by acoustic emission. Key Eng Mater 2006;312:305–10.
[4] Carpinteri A. Mechanical damage and crack growth in concrete: plastic collapse to brittle fracture. Dordrecht: Martinus Nijhoff Publishers; 1986.
[5] Carpinteri A. Decrease of apparent tensile and bending strength with specimen size: two different explanations based on fracture mechanics. Int J Solid Struct 1989;25:407–29.
[6] Carpinteri A. Scaling laws and renormalization groups for strength and toughness of disordered materials. Int J Solids Struct 1994;31:291–302.
[7] Richter CF. Elementary seismology. San Francisco and London: W.H. Freeman and Company; 1958.
[8] Gutenberg B, Richter CF. Seismicity of the earth and associated phenomena. Princeton University Press; 1949.
[9] Rundle JB, Turcotte DL, Shcherbakov R, Klein W, Sammis C. Statistical physics approach to understanding the multiscale dynamics of earthquake fault systems. Rev Geophys 2003;41:1–30.
[10] Aki K, Richards PG. Quantitative seismology: theory and methods. New York: W.H. Freeman & Co.; 1980.
[11] Carpinteri A, Chiaia B. Power scaling laws and dimensional transitions in solid mechanics. Chaos, Solitons & Fractals 1996;7:1343–64.
[12] Carpinteri A, Chiaia B. Multifractal scaling laws in the breaking behavior of disordered materials. Chaos, Solitons & Fractals 1997;8:135–50.
[13] Carpinteri A, Cornetti P. A fractional calculus approach to the description of stress and strain localization in fractal media. Chaos, Solitons & Fractals 2002;13:85–94.
[14] Carpinteri A, Pugno N, Puzzi S. Strength vs. toughness optimization of microstructured composites. Chaos, Solitons & Fractals 2009;39:1210–23.
[15] Carpinteri A, Cornetti P, Kolwankar KM. Calculation of the tensile and flexural strength of disordered materials using fractional calculus. Chaos, Solitons & Fractals 2004;21:623–32.
[16] Paggi M, Carpinteri A. Fractal and multifractal approaches for the analysis of crack-size dependent scaling laws in fatigue. Chaos, Solitons & Fractals 2009;40:1136–45.
[17] Carpinteri A, Paggi M. A fractal interpretation of size-scale effects on strength, friction and fracture energy of faults. Chaos, Solitons & Fractals 2009;39:540–6.
[18] Carpinteri A, Chiaia B, Invernizzi S. Applications of fractal geometry and renormalization group to the italian seismic activity. Chaos, Solitons & Fractals 2002;14:917–28.
[19] Carpinteri A, Cornetti P. Size effects on concrete tensile fracture properties: an interpretation of the fractal approach based on the aggregate grading. J Mech Behav Mater 2002;13:233–46.
[20] Carpinteri A, Cornetti P, Puzzi S. Scale effects on strength and toughness of grained materials: an extreme value theory approach. Strength, Fract Complex 2005;3:175–88.
[21] Stroeven P. A stereological approach to roughness of fracture surfaces and tortuosity of transport paths in concrete. Cement Concrete Comp 2000;22:331–41.
[22] Newman MEJ. Power laws, Pareto distributions and Zipf's law. Contemp Phys 2005;46:323–51.
[23] Carpinteri A, Lacidogna G, Niccolini G. Crack localisation in a large-sized R.C. beam through the acoustic emission technique. In: Proceedings of the 17th National Congress of Theoretical and Applied Mechanics (AIMETA). CD-Rom, Paper No. 23; 2005.
[24] Carpinteri A, Lacidogna G, Paggi M. Acoustic emission monitoring and numerical modelling of FRP delamination in RC beams with non rectangular cross-section. Mater Struct 2006;40:553–66.
[25] Carpinteri A, Lacidogna G, Pugno N. Structural damage diagnosis and life-time assessment by acoustic emission monitoring. Eng Fract Mech 2007;74:273–89.
[26] Spyropoulos C, Scholz CH, Shaw BE. Transition regimes for growing crack populations. Phys Rev E 2002;65:056105-1–056105-10.
[27] Carpinteri A, Lacidogna G, Niccolini G, Puzzi S. Critical defect size distributions in concrete structures detected by the acoustic emission technique. Meccanica, in press. doi:10.1007/s11012-007-9101-7.
[28] Carpinteri A, Lacidogna G, Niccolini G, Puzzi S. Morphological fractal dimension versus power-law exponent in the scaling of damaged media. Int J Damage Mech, in press.